# Identification of the Principal Binding Site for RGD-Containing Ligands in the $\alpha_V\beta_3$ Integrin: A Photoaffinity Cross-Linking Study†

Dror Yahalom,‡ Angela Wittelsberger,‡ Dale F. Mierke,§ Michael Rosenblatt,‡ Joseph M. Alexander,‡ and Michael Chorev*,‡

*Bone and Mineral Metabolism Unit, Charles A. Dana and Thorndike Laboratories, Department of Medicine, Beth Israel Deaconess Medical Center and Harvard Medical School, 330 Brookline Avenue, Boston, Massachusetts 02215, and Departments of Chemistry and Molecular Pharmacology, Division of Biology & Medicine, Brown University, Providence, Rhode Island 02912*

*Received February 18, 2002; Revised Manuscript Received May 3, 2002*

ABSTRACT: By superimposing data obtained by photo-cross-linking RGD-containing ligands to the human $\alpha_V\beta_3$ integrin onto the crystal structure of the ectopic domain of this receptor (Xiong et al. (2001) *Science 294*, 339−345), we have identified the binding site for the RGD triad within this integrin. We synthesized three novel analogues of the 49-amino acid disintegrin, echistatin: [Bpa$^{21}$,Leu$^{28}$]-, [Bpa$^{23}$,Leu$^{28}$]-, and [Bpa$^{28}$]echistatin. Each contains a photoreactive *p*-benzoyl-phenylalanyl (Bpa) residue in close proximity to the RGD motif which spans positions 24−26; together, the photoreactive positions flank the RGD motif. The analogues bind with high affinity to the purified recombinant $\alpha_V\beta_3$ integrin, but very poorly to the closely related human $\alpha_{IIb}\beta_3$ platelet integrin. While echistatin analogues containing Bpa in either position 23 or 28 cross-link specifically and almost exclusively to the $\beta_3$ subunit of $\alpha_V\beta_3$, [Bpa$^{21}$,Leu$^{28}$]-echistatin cross-links to both the $\alpha_V$ and the $\beta_3$ subunits, with cross-linking to the former favored. [Bpa$^{23}$,-Leu$^{28}$]echistatin cross-links 10−30 times more effectively than the other two analogues. We identified $\beta_3$[109−118] as the domain that encompasses the contact site for [Bpa$^{28}$]echistatin. This domain is included in $\beta_3$[99−118] (Bitan et al. (2000) *Biochemistry 39*, 11014−11023), a previously identified contact domain for a cyclic RGD-containing heptapeptide with a benzophenone moiety in a position that is similar to the placement of the benzophenone in [Bpa$^{28}$]echistatin relative to the RGD triad. Recently, we identified $\beta_3$[209−220] as the contact site for an echistatin analogue with a photoreactive group in position 45, near the C-terminus of echistatin (Scheibler et al. (2001) *Biochemistry 40*, 15117−14126). Taken together, these results support the hypothesis that the very high binding affinity of echistatin to $\alpha_V\beta_3$ results from two distinct epitopes in the ligand, a site including the RGD triad and an auxiliary epitope at the C-terminus of echistatin. Combining our results from photoaffinity cross-linking studies with data now available from the recently published crystal structure of the ectopic domain of $\alpha_V\beta_3$, we characterize the binding site for the RGD motif in this receptor.

Integrins are heterodimeric cell surface receptors which mediate cell−cellular and cell−extracellular matrix adhesion, as well as cell migration (*1*). There are at least 17 α and nine $\beta$ subunits which can combine to generate some 25 integrin subtypes, at least eight of which bind the Arg−Gly−Asp (RGD)[1] triad present in ligands (*2*, *3*). The $\alpha_V\beta_3$ integrin (vitronectin receptor) is the most abundant integrin receptor expressed by human osteoclasts, the multinucleated cells responsible for bone resorption. The $\alpha_V\beta_3$ is thought to participate in the attachment of the osteoclast to the bone matrix (*4*, *5*) and to play a crucial role in bone resorption, as demonstrated by the findings that anti-$\alpha_V\beta_3$ antibodies inhibit bone resorption in vitro (*6*) and RGD-containing antagonists of the $\alpha_V\beta_3$ receptor block bone resorption in vitro and in vivo (*5*, *7*, *8*). These studies provide "proof of concept" for novel mechanism-based approaches for the treatment and prevention of metabolic bone diseases such as osteoporosis. The involvement of the $\alpha_V\beta_3$ integrin in other critical processes, such as metastasis and angiogenesis (*9*), also suggests the potential therapeutic significance of potent antagonists in pathologies other than metabolic bone diseases.

† This work was supported in part by Grant AR42833 from NIAMS of the National Institutes of Health and a postdoctoral fellowship grant from the Deutscher Akademischer Austauschdienst to A.W.

* Corresponding author. Address: Beth Israel Deaconess Medical Center, 330 Brookline Ave. (HIM 944), Boston, MA 02215. Telephone: 617 667-0901. Fax: 617 667-4432. E-mail: michael_chorev@hms.harvard.edu.

‡ Beth Israel Deaconess Medical Center and Harvard Medical School.

§ Brown University.

[1] Abbreviations used: Acm, acetamidomethyl; Boc, *tert*-butyloxycarbonyl; BP, benzophenone; Bpa, p-benzoyl-phenylalanyl; DCC, N,N′-dicyclohexylcarbodiimide; DTT, dithiothreitol; EDTA, ethylenediaminetetraacetic acid; Endo-F, endoglycosidase-F/N-glycosidase F; ESI-MS, electrospray ionization mass spectra; Glu-C, endoproteinase Glu-C; HEK, human embryonic kidney; HOBT, 1-hydroxybenzotriazole; Lys-C, endoproteinase Lys-C; mAb, monoclonal antibodies; MIDAS, metal-ion dependent adhesion site; NMR, nuclear magnetic resonance; PAGE, polyacrylamide gel electrophoresis; PAM, *p*-(oxymethyl)-phenyacetamidomethyl resin; *p*Bz$_2$, *p*-benzoyl-benzoyl; PAS photoaffinity scanning; PBS, phosphate-buffered saline; PEG, poly(ethylene glycol); RGD, arginyl-glycyl-aspartyl; RP-HPLC, reverse-phase high-performance liquid chromatography; SDS, dodecyl sulphate sodium salt; TCEP−HCI, tris(2-carboxyethyl)phosphine hydrochloride; TFA, trifluoroacetic acid.

10.1021/bi025690t CCC: $22.00 
Published on Web 06/07/2002

Given the large size and the heterodimeric and membrane-embedded nature of the intact $\alpha_V\beta_3$ receptor, the integrin is not easily amenable to high-resolution structural analyses, such as single-crystal X-ray and nuclear magnetic resonance. But recently, Xiong and co-workers succeeded in generating a crystal structure of the extracellular portion of integrin $\alpha_V\beta_3$ (*10*). The structure shows a "head" with two rodlike tails from the $\alpha_v$ and $\beta_3$ subunits, including a putative flexible hinge region ("genu"). The main components of the head are a seven-bladed $\beta$-propeller domain in $\alpha_V$ and the A-domain of $\beta_3$, with the contact surface between these domains being the major interface between the two receptor subunits.

The ligand-binding site, however, still remains to be elucidated. The major interactions between $\alpha_V\beta_3$ and its endogenous ligands is based on a three-amino-acid sequence, RGD, displayed on the ligand. Some ligand-binding regions have been proposed on the basis of site-directed mutagenesis or studies with naturally occurring $\beta_3$ mutants. Two ligand-binding elements are proposed to lie in the $\alpha_V$ subunit within the $\beta$-propeller domain. In $\beta_3$, the metal ion-dependent adhesion site (MIDAS) residues D119, S121, S123, E220, R214, and D217 have been shown to be involved in ligand-binding (*11*).

The main advantage of the photoaffinity scanning (PAS) methodology is that it generates direct evidence for the location of contact sites between ligand and receptor (*12*). Furthermore, PAS enables mapping the bimolecular interface between the ligand and receptor when the receptor is in its ligand-bound conformation. Therefore, information gathered from PAS can be very valuable in constructing an experimentally based model of a ligand−receptor complex. Such models were recently reported for the parathyroid hormone (*13*−*16*), vasopressin (*17*), secretin (*18*, *19*), motilin (*20*), and cholecystokinin receptors (*21*).

Using benzophenone (BP) as a photoreactive moiety for PAS, we previously identified two contact sites between the $\alpha_V\beta_3$ receptor and two BP-substituted cyclic RGD-containing heptapeptides. When the photoreactive moiety is positioned C-terminal to RGD, the peptide cross-links within the sequence 99−118 on the $\beta_3$ subunit of the receptor, whereas the corresponding peptide with a photoreactive group N-terminal to RGD cross-links to $\beta_3$[167−171] (*22*, *23*). In both cases, cross-linking occurs to the $\beta_3$ chain almost exclusively (>95%) with negligible labeling of the $\alpha_V$ chain. Both of these contact sites are located in the A-domain of the $\beta_3$ (previously referred to as the I-like domain).

To gain further insights into the mode of interaction of the $\alpha_V\beta_3$ receptor with much larger, highly potent, and more selective RGD-containing ligands, we used a member of the disintegrin family, echistatin, as the ligand for additional photoaffinity cross-linking studies. This small protein was originally isolated from the venom of the snake *Echis carinatus* (*24*) and binds with high affinity to $\alpha_V\beta_3$ and $\alpha_{IIb}\beta_3$ integrins. There is a considerable amount of structural information known about echistatin. NMR studies of the 49-amino acid protein reveal a rigid globular fold stabilized by four disulfide bridges, a $\beta$-hairpin motif with a flexible loop region, and a flexible C-terminal sequence (*25*, *26*). The RGD triad is located in the mobile loop at the tip of the hairpin and has been shown to be important for tight binding of echistatin to $\alpha_V\beta_3$ (*27*, *28*). The flexible C-terminal sequence of echistatin is believed to contribute substantially to the binding affinity by providing an auxiliary site that interacts with an exosite on the receptor distinct from the RGD-binding elements. Indeed, deletion of this C-terminal region generates a truncated echistatin with decreased binding to $\alpha_V\beta_3$ and $\alpha_{IIb}\beta_3$ (*28*). A linear peptide segment of this region, echistatin[40−49], inhibits binding of echistatin to $\alpha_{IIb}\beta_3$ (*29*). Recently, we identified a contact site between the human $\alpha_V\beta_3$ receptor and the C-terminus of echistatin (*30*). We cross-linked the potent radioiodinated echistatin analogue, $^{125}$I-[Arg$^{35}$,Lys$^{45}$($N^{\epsilon}$-*p*Bz$_2$)]echistatin ($^{125}$I−K$^{45}$(BP)-echistatin), which carries a photophore on Lys$^{45}$ at the far C-terminal region of echistatin, and subsequently characterized the ligand−receptor conjugate. A short sequence of twelve amino acids ($\beta_3$[209−220]) was revealed to contain the contact site. This putative auxiliary contact site for echistatin differs from the two contact domains ($\beta_3$[99−118] and $\beta_3$[167−171]) identified previously for BP-substituted positions flanking the RGD triad in two cyclic heptapeptides (*22*, *23*).

In this study, we report the design and synthesis of three new echistatin analogues, each incorporating a single BP-containing amino acid residue at either positions 21, 23, or 28, in immediate proximity to the R$^{24}$GD$^{26}$ triad. Positions 21 and 28 correspond to the BP-substituted positions in the short cyclic RGD-containing ligands employed in previous PAS studies (*22*, *23*). The three analogues, [Bpa$^{21}$,Leu$^{28}$]-, [Bpa$^{23}$,Leu$^{28}$]-, and [Bpa$^{28}$]echistatin, were found to bind with high affinity to the purified $\alpha_V\beta_3$ integrin. The radioiodinated analogues cross-link effectively and specifically to the recombinant human $\alpha_V\beta_3$ receptor stably expressed by human embryonic kidney (HEK)-293 cells. The mode of photo-cross-linking differed in the three analogues, not only with respect to efficiency, but also with regard to the contact region on the receptor. We present data comparing photo-cross-linking characteristics of the three analogues and a detailed analysis identifying the contact domain for [Bpa$^{28}$]-echistatin. An emerging experimentally based model of the ligand−$\alpha_V\beta_3$ integrin bimolecular interface is described, taking advantage of the recently published crystal structure of the ectopic portion of the $\alpha_V\beta_3$ integrin. Superimposition of the contact domains, delineated by photoaffinity cross-linking, on the X-ray crystal structure of the $\alpha_V\beta_3$ ectopic domain provided guidance for docking echistatin by molecular modeling and allowed the location of the RGD binding site to be identified.

## EXPERIMENTAL PROCEDURES

*Materials.* HEK293 cells stably expressing the human $\alpha_V\beta_3$ integrin receptor were a generous gift from Drs. Le Duong, S. Rodan, and G. Rodan (Merck Research Laboratories, West Point, PA). Outdated platelets were obtained from the Beth Israel Deaconess Medical Center Blood Bank (Boston, MA). [Leu$^{28}$]echistatin was a generous gift from Dr. R. J. Gould (Merck, West Point PA). Amino acid derivatives and peptide synthesis reagents were purchased from PE-Biosystems (Framingham, MA). TCEP was from Pierce (Rockford, IL). Na$^{125}$I was obtained from Amersham-Pharmacia (Arlington Heights, IL). Sequencing-grade endoproteinase Arg-C and endoproteinase Glu-C were obtained from Roche Diagnostics (Indianapolis, IN). Sequencing-grade endoproteinase Lys-C was purchased from Sigma (St. Louis,

MO). Endoglycosidase F (PNGase F) was obtained from New England BioLabs (Beverly, MA). Tissue culture media were from Gibco-BRL (Gaithersburg, MD). All tissue culture disposables and plasticware were from Corning (Corning, NY). All other chemical reagents were of the highest analytical grade available and were purchased from Aldrich/Sigma/Fluka Group (St. Louis, MO).

Electrospray ionization-mass spectra (ESI-MS) were recorded on a Micromass Platform LCZ system equipped with an electrospray ionization source and a Waters 2690 Separation Module. For analytical and preparative RP-HPLC, Vydac C18 columns from The Separation Group (Hesparia, CA) were used; the solvent system used was water/TFA (1000:1, eluent A) and acetonitrile/TFA (1000:1, eluent B). Linear elution gradients were used ("Waters Gradient 6") unless otherwise stated. Flow rates were 0.2 mL/min for analytical and 20 mL/min for preparative RP-HPLC; product elution was monitored at 220 nm.

*Synthesis of [Bpa[28]]Echistatin.* The synthesis was performed as previously described for K[45](BP)-echistatin (*30*). The linear precursor of the echistatin analogue was synthesized by automated solid-phase methodology on an Applied Biosystems 430A peptide synthesizer using Boc/HOBt/DCC chemistry. Bpa (*p*-benzoyl-phenylalanine) was introduced as Boc-Bpa-OH, and its coupling was manually monitored by a ninhydrin test (*31*). Cysteine side chains were Acm protected, while all other residues were protected in the standard manner compatible with liquid HF cleavage and deprotection protocols. The peptide was assembled on 0.12 mmol Boc−Thr(Bzl)−PAM resin (loading: 0.7 mmol/g). Residues were incorporated by a double coupling protocol (2 mmol of activated amino acid derivative per cycle) followed by a capping step with acetic anhydride. The quality of the individual coupling steps was occasionally monitored by the ninhydrin test (*31*). The product was cleaved from the resin by liquid HF in the presence of 10% anisole at 0 °C and purified by ether precipitation and RP-HPLC (gradient 0%-50%B in 120 min) followed by lyophilization.

The partially protected (*S*-Acm) linear precursor (55 mg, 9.0 $\mu$mol) was dissolved in MeOH/water (9 mL, 2/1 v/v), and methoxycarbonylsulfonyl chloride (200 $\mu$L, 1.5 mmol) was added under ice-cooling. After 25 min, the entire solution was subjected to a RP-HPLC separation (gradient 0%-50%B in 120 min). The isolated *S*-methoxycarbonylsulfonyl-protected linear precursor (28 mg, 4.7 $\mu$mol) was dissolved in water (5 mL), and tris-(2-carboxyethyl)phosphine hydrochloride (TCEP·HCl) (100 mg, 0.35 mmol) was added. After 30 min, the solution was injected into the RP-HPLC (gradient 0%-50%B in 120 min), and the eluted product was immediately lyophilized. The reduced analogue (~25 mg) was then dissolved in 0.07 M $NH_4OAc$ buffer (500 mL, pH 8.0) and stirred for 24h at 4 °C, followed by 2d at room temperature. Final purification of the oxidized material was achieved by RP-HPLC (gradient 0%-50%B in 120 min), and the product was characterized by ESI-MS and amino acid analysis. MW: calculated, 5537; found, 5537 (based on the $[M+7H]^{+7}$ $m/e = 792$). Analytical RP-HPLC: $R_T = 12.49$ min, gradient 10−50%B in 30 min. Amino acid analysis (calculated): Asx 7.8 found (8), Thr 2.4 (3), Ser 0.6 (1), Glx 2.7 (3), Pro 4.8 (4), Gly 4.8 (5), Ala 2.0 (2), Ile 0.8 (1), Leu 0.9 (1), Tyr 0.8 (1), Phe 0.9 (1), His 1.0 (1), Lys 4.6 (5), Arg 3.8 (4)).

*Synthesis of [Bpa[21],Leu[28]]Echistatin, [Bpa[23],Leu[28]]Echistatin.* The linear partially protected (Cys residues protected with *S*-Acm) precursors of these echistatin analogues were synthesized, purified and analyzed by AusPep (Parkville, Australia). (For [Cys[2,7,8,11,20,32,37,39](*S*-Acm),Bpa[21],Leu[28]]echistatin, MW: calculated 6099. Matrix-assisted laser desorption mass spectra−time-of-flight (MALDI-TOF) MW found: 6099.0. Analytical RP-HPLC (Merck, Darmstadt) Supersphere, 250-4, LiChrocart 100 RP-18: $R_T = 26.13$ min, linear gradient 0−70%B in 35 min ($A = 0.1\%$ TFA in water; $B =$ 0.09% TFA in acetonitrile/$H_2O$ 1:1), flow rate 1 mL/min, and monitored at 218 nm. Amino acid analysis (calculated): Asx 8.7 (8), Thr 2.6 (3), Ser 0.9 (1), Glx 2.6 (3), Pro 4.0 (4), Gly 5.0 (5), Ala 2.2 (2), Ile 0.8 (1), Leu 2.2 (2), Tyr 0.7 (1), Phe 0.9 (1), His 1.0 (1), Lys 4.0 (4), Arg 4.1 (4). For [Cys[2,7,8,11,20,32,37,39](*S*-Acm),Bpa[23],Leu[28]]echistatin, MW: calculated, 6157; found, 6157.4. Analytical RP-HPLC: $R_T =$ 24.37 min. Amino acid analysis (calculated): Asx 8.1 (8), Thr 2.7 (3), Ser 0.9 (1), Glx 2.9 (3), Pro 3.9 (4), Gly 4.9 (5), Ala 1.1 (1), Ile 0.9 (1), Leu 2.0 (2), Tyr 1.3 (1), Phe 1.0 (1), His 1.1 (1), Lys 5.0 (5), Arg 4.1 (4). The linear peptides were subjected to the reduction−oxidation process described above for [Bpa[28]]echistatin. The products were characterized by ESI-MS. ([Bpa[21],Leu[28]]echistatin. MW: calculated, 5522; found, 5520 (based on the $[M+5H]^{+5}$ $m/e = 1105$). Analytical RP-HPLC: $R_T = 12.35$ min, gradient 10−50%B in 30 min. [Bpa[23],Leu[28]]echistatin. MW: calculated, 5580; found, 5580 (based on the $[M+5H]^{+5}$ $m/e = 1117$). Analytical RP-HPLC: $R_T = 11.89$ min, gradient 10%-50%B in 30 min.)

*Radioiodination of Echistatin and Echistatin Analogues.* Radioiodination was achieved by the lactoperoxidase method (*32*). The peptide (35−50 $\mu$g, 6−9 nmol) was dissolved in 0.1 M sodium phosphate buffer pH 7.4 (100 $\mu$L). Lactoperoxidase (0.2 units) in sodium phosphate buffer (20 $\mu$L) was added to the dissolved peptide (50 $\mu$L), followed by 2 mCi $Na^{125}I$ in a NaOH solution. Four aliquots (3 $\mu$L each) of $H_2O_2$ (0.003%) were added every 3 min. The resulting solution was subjected to RP-HPLC purification. Gradient: linear gradient 12−20%B (echistatin) or 20−32%B (echistatin analogues) in 30 min. The 1 mL fractions were diluted by adding 1% (w/v) BSA (0.1 mL) solution. The isolated radioactive peaks were stored at −80 °C until use for either binding studies or photoaffinity cross-linking experiments.

*Radioreceptor Competition Binding Assay*. The affinity of the peptides for purified human integrin $\alpha_V\beta_3$ was measured in a radioreceptor competition binding assay with $^{125}$I-echistatin as tracer in binding buffer (25 mM Tris/HCl, pH 7.4, 150 mM NaCl, 1 mM $CaCl_2$, 1 mM $MgCl_2$, and 1% BSA), as previously reported (*33*).

*Photoaffinity Cross-Linking to HEK-293 Cells Stably Expressing Human Integrin $\alpha_V\beta_3$.* In a typical preparative-scale cross-linking experiment, $^{125}$I−[Bpa[28]]echistatin (~$10^8$ cpm, ~20 pmol) was photo-cross-linked to HEK-293 cells stably expressing recombinant human integrin $\alpha_V\beta_3$ at ~$10^6$ copies/cell (harvested from 10 confluent 75 cm$^2$ plates, ~9 nmol $\alpha_V\beta_3$ receptor/plate) according to a published protocol (*22*) in the presence of 1mM $MgCl_2$ and 1 mM $MnCl_2$. Following cross-linking, the cells were washed 3 times with phosphate-buffered saline (PBS), lysed by 30 min incubation with 10 mL M-PER (Pierce, Rockford, Il), and reduced with dithiothreitol (DTT), and the Cys residues were alkylated with iodoacetamide as previously described (*13*). The

reduced and alkylated ligand−receptor photoconjugate was purified by preparative SDS−PAGE. Several batches of photoconjugate showed consistency in resulting digestions. For comparative studies, corresponding cross-linking experiments with all three Bpa-containing echistatin analogues were performed on a smaller scale.

*Enzymatic and Chemical Digestions*. Enzymatic and chemical digestions were performed according to the protocols published by Bisello et al. (*13*) and Bitan et al. (*23*). CNBr digestions were performed both in solution and on solid-phase, as described in the above references, and generated identical results. Digestions using endoproteinase Glu-C were performed in 100 mM ammonium acetate buffer pH 4 (34). These digestions were performed at room temperature for 18 h, unless otherwise stated.

*Platelet Binding Assay.* Outdated platelets were centrifuged at 1500 rpm for 20 min; the pellet was than washed 3 times with Tyrode's buffer (134 mM NaCl, 3 mM KCl, 0.3 mM $NaH_2PO_4$, 2 mM $MgCl_2$, 5 mM HEPES, 7.5% w/v $NaHCO_3$, 0.35% BSA, 0.1% D-glucose, pH 7.4), followed by centrifugation each time at 1500 rpm for 20 min. The pellet was resuspended in Tyrode's buffer adjusted to the concentration of $1 \times 10^6$ platelets/mL. The affinity of the peptides for the platelet integrin $\alpha_{IIb}\beta_3$ was measured in a radioreceptor competition binding assay with $^{125}$I-echistatin as tracer, similar to the one performed for the integrin $\alpha_V\beta_3$. A 200 $\mu$L sample of the above platelet preparation was mixed with $^{125}$I-echistatin (25 $\mu$L, ~150 000 cpm) and the relevant peptide (25 $\mu$L, in Tyrode's buffer). Following 1 h incubation at room temperature, the cells were filtered on a fiberglass filtermat using the Skatron combi cell harvester (Skatron Instruments Inc., Sterling, VA). The filters were counted in a GammaTrac 1193 counter (TM Analytic Inc., Elk Grove Village, IL). Nonspecific binding was determined by incubating the radioligand and cells in the presence of excess (10 $\mu$M) echistatin.

*Platelet Cross-Linking.* Outdated platelets were washed as above. The final concentration of cells was adjusted to give similar receptor numbers as those in the parallel assay with HEK293 cells stably expressing the $\alpha_V\beta_3$ integrin receptor. Cross-linking of the analogues to the platelets was carried out following the identical protocol as described for $\alpha_V\beta_3$-expressing cells.

*Molecular Modeling*. The starting conformation of $\alpha_V\beta_3$ (pdb: 1JV2) was derived from the recently published X-ray structure (*10*). The model of the binding site of echistatin consisted of $\alpha_V$[F1-A437] and $\beta_3$[N99−R352] from the X-ray structure. The NMR-derived structure of echistatin (pdb: 2ECH) was used in the modeling of the complex (*26*).

To model the interaction between $\alpha_V\beta_3$ and echistatin, the ligand was placed to satisfy the photoaffinity labeling contact points: $\beta_3$[169−171], $\beta_3$[109−118], and $\beta_3$[209−220] to Lys$^{21}$, Met$^{28}$, and Lys$^{45}$ in echistatin, respectively. The C-terminus of echistatin was rotated away from the RGD-containing loop by a ca. 120° rotation about the backbone dihedral angles of Arg$^{41}$ and Asn$^{42}$. This was necessary to place the C-terminus of echistatin in proximity to $\beta_3$[209−220]. To examine the fulfillment of the contact points, we applied distance constraints to the Cα atoms of residues within these regions of $\beta_3$ with a target distance of 12 Å. This lenient distance was chosen to account for the placement of the Bpa residue used for the photoaffinity labeling experiments. The resulting model was then relaxed (energy minimized) and followed by extensive molecular dynamics (MD) simulations using the CVFF91 force field module within the Discover program (Molecular Simulations, Inc., San Diego, CA). Additional MD simulations were carried out with application of template forcing to the original Cartesian coordinates of the X-ray structure of $\alpha_V\beta_3$ and/or NMR structure of echistatin.

## RESULTS

*Synthesis of Echistatin Analogues.* The three echistatin analogues [Bpa$^{21}$,Leu$^{28}$]-, [Bpa$^{23}$,Leu$^{28}$]-, and [Bpa$^{28}$]echistatin were obtained in good yield and high purity, as shown by mass spectrometric, HPLC, and amino acid analyses. The linear Acm-protected precursor of [Bpa$^{28}$]echistatin was synthesized by us, whereas the two Acm-protected linear precursors of [Bpa$^{21}$,Leu$^{28}$]- and [Bpa$^{23}$,Leu$^{28}$]echistatin were synthesized and characterized by mass spectrometry and amino acid analysis by AusPep (Parkville, Australia). The Acm protecting group was exchanged to the more labile S-methoxycarbonylsulfonyl group before reduction to free cysteine side-chains. The final folded molecules formed spontaneously during air oxidation, as observed previously (*30*). The reference peptide [Leu$^{28}$]echistatin was kindly provided by Dr. R. J. Gould (Merck, West Point PA).

*Affinities of Echistatin Analogues Toward the $\alpha_V\beta_3$ and the $\alpha_{IIb}\beta_3$ Integrin Receptors.* The competition binding curves of [Bpa$^{21}$,Leu$^{28}$]echistatin, [Bpa$^{23}$,Leu$^{28}$] echistatin, [Bpa$^{28}$] echistatin, [Leu$^{28}$]echistatin, and the unsubstituted echistatin to the $\alpha_V\beta_3$ and the $\alpha_{IIb}\beta_3$ integrin receptors were measured in the presence of $^{125}$I-echistatin and are reported in panels A and B, respectively, of Figure 1. The three Bpa-containing analogues bound with 10−100-fold reduced affinity to purified $\alpha_V\beta_3$ integrin compared to echistatin and the reference peptide [Leu$^{28}$]echistatin. The binding properties for the $\alpha_{IIb}\beta_3$ integrin receptor were different than those for $\alpha_V\beta_3$, despite both receptors sharing the identical $\beta_3$ subunit (Figure 1, B). All tested compounds showed a reduced binding affinity to $\alpha_{IIb}\beta_3$ compared to $\alpha_V\beta_3$. The affinity of echistatin itself was about 100-fold weaker, whereas the affinity of [Leu$^{28}$]echistatin was at least 1000-fold weaker, and the Bpa-modified analogues showed no significant binding.

*Cross-Linking of Radioiodinated Echistatin Analogues to the $\alpha_V\beta_3$ Integrin Receptor*. The echistatin analogues [Bpa$^{21}$,-Leu$^{28}$]echistatin (**5**), [Bpa$^{23}$,Leu$^{28}$]echistatin (**6**), and [Bpa$^{28}$]-echistatin (**7**) were radioiodinated using the lactoperoxidase method (*32*). The radiolabeled compounds were then cross-linked to HEK293 cells stably expressing the $\alpha_V\beta_3$ receptor (~$10^6$ receptors/cell) by photoirradiation at 365 nm. After extraction, the ligand−receptor conjugates were reduced, cysteine side chains were alkylated, and the conjugates were purified by SDS−PAGE. An SDS−PAGE analysis of the purified cross-linked conjugates is represented in Figure 2A. All three analogues cross-linked specifically to the receptor within the binding site of echistatin. Cross-linking to the parental HEK293 cells (which do not express $\alpha_V\beta_3$) was not observed (data not shown), and cross-linking to cells expressing the $\alpha_V\beta_3$ receptor was inhibited in the presence of unlabeled echistatin, as shown in Figure 2A (lanes 2, 4, and 6, for [Bpa$^{21}$,Leu$^{28}$]-, [Bpa$^{23}$,Leu$^{28}$]-, and [Bpa$^{28}$]-

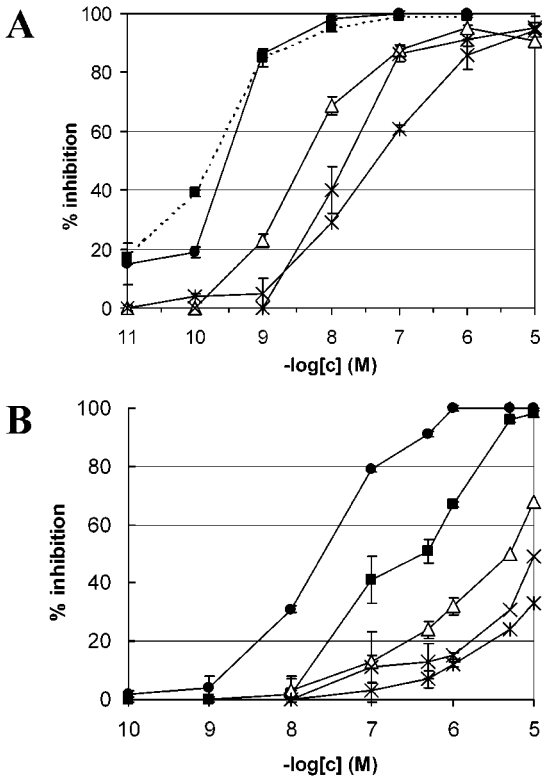


FIGURE 1: Competition of $^{125}$I-echistatin binding to the purified human $\alpha_V\beta_3$ receptor (A) and to platelets expressing the human $\alpha_{IIb}\beta_3$ integrin (B) with echistatin (●), [Leu$^{28}$]echistatin (■), [Bpa$^{21}$,-Leu$^{28}$]echistatin (**5**) (△), [Bpa$^{23}$,Leu$^{28}$]echistatin (**6**) (×), and [Bpa$^{28}$]-echistatin (**7**) (∗). The data point represents the mean ± SEM of three independent experiments performed in triplicates.

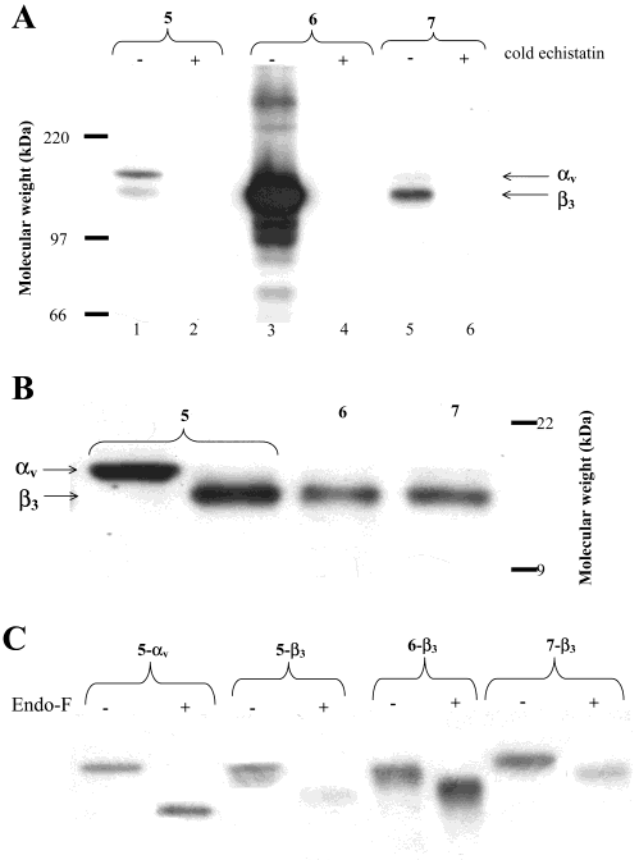


FIGURE 2: (A) Autoradiograph of an SDS−PAGE analysis of the conjugates obtained by photo-cross-linking of the $^{125}$I-labeled Bpa-containing echistatin analogues **5**−**7** to HEK293 cells expressing recombinant human $\alpha_V\beta_3$ receptor (~$10^6$ receptors/cell). Lanes 2, 4, and 6 show the inhibition of the cross-linking in the presence of excess (1$\mu$M) unlabeled echistatin. The arrows indicate the bands corresponding to cross-linking to the $\alpha_V$ or the $\beta_3$ subunit of the integrin. (B) SDS−PAGE analysis of the purified radiolabeled conjugated bands. The autoradiographs are representatives of three reproducible independent experiments. (C) Endo-F digestion of the purified radiolabled conjugated bands obtained after photoaffinity cross-linking to HEK-293 cells expressing the recombinant human $\alpha_V\beta_3$ receptor. The autoradiograph is a representative of three reproducible independent experiments.

echistatin, respectively). As demonstrated by the differences in intensity of the photoconjugated radiolabeled bands, the yield of cross-linking of the Bpa$^{23}$-analogue (**6**) was 10−30 times higher than that of the Bpa$^{21}$- and the Bpa$^{28}$-modified analogues. [Bpa$^{21}$,Leu$^{28}$]echistatin (**5**) cross-links to both the $\alpha_V$ and the $\beta_3$ subunit of the receptor, and to a greater extent to the former (lane 1, Figure 2A). This finding is in contrast not only to the cross-linking site of [Bpa$^{23}$,Leu$^{28}$]echistatin (**6**) and [Bpa$^{28}$]echistatin (**7**), but also to the previously identified cross-linking sites for K$^{45}$(BP)-echistatin (*30*) and the heptapeptidic cyclic RGD-containing ligands (*22*, *23*). All of these BP-containing ligands cross-link almost exclusively (>95%) to the $\beta_3$ subunit. A comparison of the purified (excised and eluted) photoconjugated radiolabeled bands of all three Bpa-containing echistatin analogues (**5**−**7**) demonstrates the distinctive and efficient cross-linking of [Bpa$^{21}$,Leu$^{28}$]echistatin (**5**) to the $\alpha_V$-subunit (Figure 2B).

Treatment of the purified radiolabeled ligand−receptor photoconjugates with endoglycosidase F/N-glycosidase F (Endo-F) shifts their radiolabeled bands to lower molecular weights, indicating that the conjugates are glycosylated (Figure 2, C). Specifically, the band of the [Bpa$^{21}$,Leu$^{28}$]echistatin−$\alpha_V$ conjugate shifts from ~160 to ~110 kDa, which is consistent with $\alpha_V$ being highly glycosylated (*35*). The $\beta_3$-containing conjugate bands are less heavily glycosylated, as evidenced by shifts from ~130 to ~110 kDa.

*Photoaffinity Cross-Linking of [Bpa$^{28}$]Echistatin to the $\alpha_v\beta_3$ and the $\alpha_{IIb}\beta_3$ Integrin Receptors.* The most abundant integrin receptor on platelets is the $\alpha_{IIb}\beta_3$ integrin, which shares a common $\beta$ subunit with $\alpha_V\beta_3$ but contains a different $\alpha$ subunit. To examine the cross-linking specificity of $^{125}$I-[Bpa$^{21}$,Leu$^{28}$]echistatin, $^{125}$I-[Bpa$^{23}$,Leu$^{28}$]echistatin, and $^{125}$I-[Bpa$^{28}$]echistatin, we compared their photo-cross-linking to HEK293 cells stably expressing the $\alpha_V\beta_3$ receptor with photo-cross-linking to outdated human platelets. The cross-linking efficiency to the $\alpha_{IIb}\beta_3$ integrin was found to be much lower than that to the $\alpha_V\beta_3$ integrin, as shown in lanes 2, 4, and 6 of Figure 3. Efficient cross-linking with $\alpha_{IIb}\beta_3$ was obtained solely for the Bpa$^{23}$ analogue, which showed a considerably higher cross-linking efficiency than the other two analogues for $\alpha_{IIb}\beta_3$. This observation corresponds to the higher cross-linking efficiency of the Bpa$^{23}$ analogue to the $\alpha_V\beta_3$ receptor. Of note, the sample concentration for [Bpa$^{23}$,Leu$^{28}$]echistatin used in the SDS−PAGE analysis of Figure 3 was 10-fold lower than the concentration used for the other two analogues. The reduced cross-linking efficiency of all three analogues to $\alpha_{IIb}\beta_3$ is consistent with the low binding affinity to the same receptor.

We undertook a more detailed analysis of the photoconjugate obtained with [Bpa$^{28}$]echistatin (**7**). The position of the Bpa photophore relative to the RGD triad in [Bpa$^{28}$]-

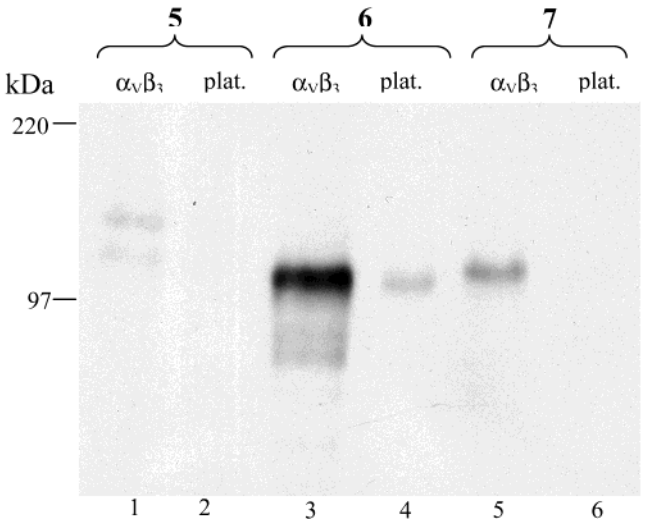


FIGURE 3: Autoradiograph of an SDS−PAGE analysis of the photoaffinity cross-linking of the $^{125}$I-labeled Bpa-containing echistatin analogues **5**, **6**, and **7** to HEK-293 cells expressing recombinant human $\alpha_V\beta_3$ receptor (lanes 1, 3, and 5) compared to platelets expressing predominantly the $\alpha_{IIb}\beta_3$ receptor (lanes 2, 4, and 6). The autoradiograph is a representative of three reproducible independent experiments.

echistatin is identical to the placement of Bpa in the small RGD-containing peptide **1**. $\beta_3$[99−118] was found to comprise the contact site for peptide **1** (*22*). The availability of [Bpa[28]]echistatin offered an opportunity to compare a small RGD-containing peptide with a disintegrin for their interaction with the same integrin receptor.

*Identification of the Contact Site on the $\alpha_V\beta_3$ Integrin Receptor for [Bpa[28]]Echistatin.* The purified radiolabeled photo-cross-linked conjugate between the $\alpha_V\beta_3$ receptor and [Bpa[28]]echistatin (**7**) was analyzed after enzymatic and chemical digestions in order to determine the cross-linking site in the receptor. Enzymatic digestions included treatment with endoproteinase Lys-C, endoproteinase Arg-C, and endoproteinase Glu-C, cleaving at the carboxyl side of lysine, arginine, and glutamic acid residues, respectively. Chemical digestion with cyanogen bromide was used for cleaving the conjugate at the carboxyl side of methionine residues. Upon treatment of the [Bpa[28]]echistatin−receptor conjugate with Lys-C, the ∼130 kDa-band of the intact photoconjugate yielded a 7 kDa radiolabeled band (Figure 4A, lane 3). Isolation of this band and subsequent treatment with Endo-F generated a radiolabeled band of ∼3.5 kDa (Figure 4A, lane 4), demonstrating the Lys-C cleavage product to be glycosylated. After subtraction of the molecular weight contributed by the conjugated portion of the ligand, the theoretical Lys-C cleavage map of the $\beta_3$ subunit suggests three possible regions, $\beta_3$[99−125], $\beta_3$[355−384], and $\beta_3$[533−580], as putative cross-linked fragments that are consistent in size with the experimentally found ∼3.5 kDa ligand−$\beta_3$ conjugate fragment.

Exposure of the intact conjugate to Arg-C yielded a ∼9 kDa fragment in addition to higher molecular weight bands resulting from incomplete digestion (Figure 4A, lane 5). When treated with Endo-F, the electrophoretic mobility of the 9 kDa band was not altered, showing that it is not glycosylated. Treating the deglycosylated ligand−receptor photoconjugate with Arg-C (data not shown) generated a similar size band. The theoretical map for Arg-C cleavage

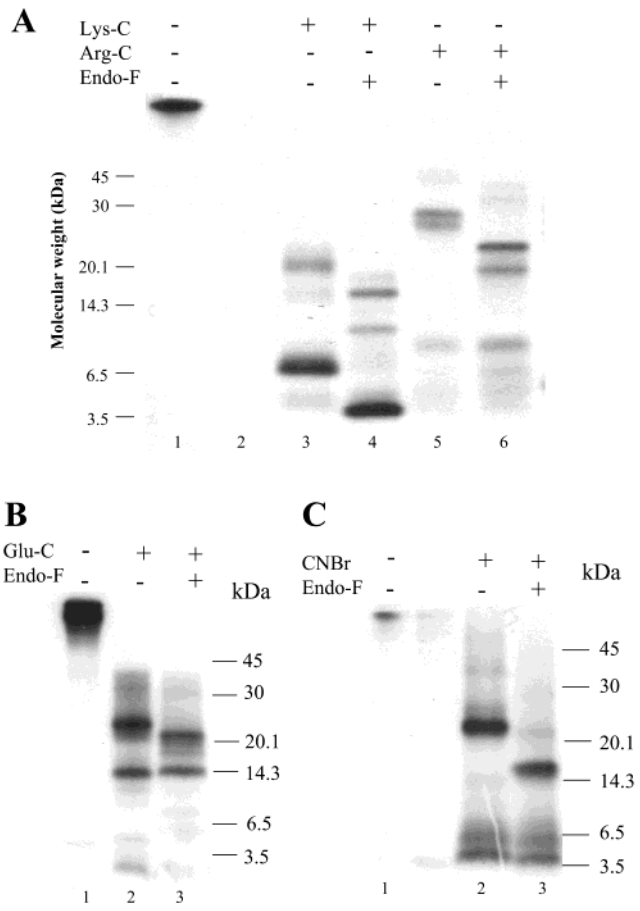


FIGURE 4: A. Digestions of the $\beta_3$-**7** photoconjugate by Lys-C, Arg-C, and secondary digestions by Endo-F. Lane 1: Intact $\beta_3$-**7** photoconjugate. Lane 3: Digestion by Lys-C. Lane 4: Secondary digestion of the purified product of the Lys-C digestion with Endo-F. Lane 5: Digestion by Arg-C. Lane 6: Secondary digestion of the purified product of the Arg-C digestion with Endo-F. Samples were analyzed by 16.5% w/v Tricine/SDS−PAGE. The autoradiograph is a representative of three reproducible independent experiments. And digestions of the $\beta_3$-**7** photoconjugate by Glu-C (B) and by CNBr (C), with and without subsequent secondary digestion by Endo-F. Lane 1: Intact $\beta_3$-**7** photoconjugate. Lane 2: Digestion by Glu-C. Lane 3: Secondary digestion of the purified product of the Glu-C digestion with EndoF. Samples were analyzed by 16.5% w/v Tricine/SDS−PAGE. The autoradiographs are representatives of three reproducible independent experiments. Molecular weight markers are shown on the right of the autoradiograph.

identifies 10 nonglycosylated fragments that lie within 2 kDa of the experimentally found ∼9 kDa Arg-C generated ligand−$\beta_3$ photoconjugated fragment. Of these, only two ($\beta_3$-[106−143] and $\beta_3$[579−622]) overlap with the previously identified fragments generated by Lys-C cleavage. The potential contact sites consistent with sequences delimited by Lys-C, Arg-C, and Endo-F cleavages are therefore reduced to the $\beta_3$[106−125] or $\beta_3$[579−580] regions. Enzymatic digestion with Glu-C gave rise to a 15 kDa band, the product of exhaustive digestion, as well as a 23 kDa band from incomplete digestion (Figure 4B). While the band representing the incomplete digestion shifted from 23 to 21 kDa, the 15 kDa band showed no altered mobility after treatment with Endo-F and is therefore not glycosylated. Of two potential fragments identified on the Glu-C digestion map that are consistent with a 15 kDa nonglycosylated fragment, only $\beta_3$[109−171] overlaps the potential $\beta_3$[106−

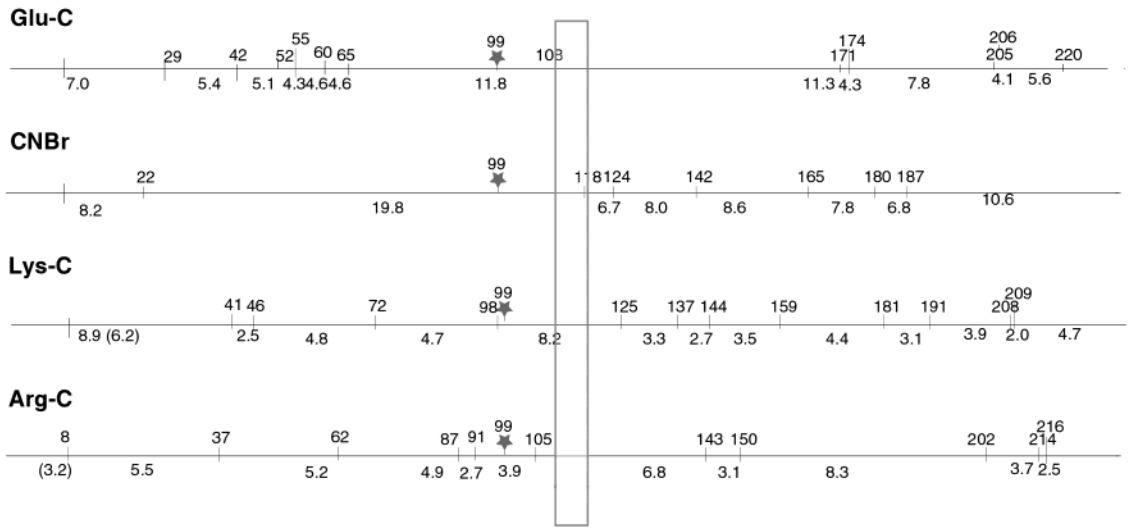


FIGURE 5: Theoretical digestion map for digestions by Glu-C, CNBr, Lys-C, and Arg-C of the region between residues 1 and 220 of $\beta_3$. A star indicates glycosylation sites. Numbers on top indicate the sites were cleavage occurs. Numbers on bottom indicate the molecular weight of the respective fragment obtained by cleavage at the two adjacent cleavage sites. Vertical box indicates the overlapping sequence identified as the contact domain for Bpa[28], a position removed 2 residues from the C-terminus of RGD.

125] contact site suggested by the combination of the Lys-C and Arg-C digestions. The only putative site of [Bpa[28]]-echistatin cross-linking consistent with the fragmentation pattern generated by the sum of all enzymatic digestions employed is the sequence $\beta_3$[109−125].

Chemical digestion of the [Bpa[28]]echistatin−receptor photoconjugate with cyanogen bromide resulted in a ~25 kDa band which shifts to ~17 kDa upon exposure to Endo-F (Figure 4 C). From the theoretical digestion map of $\beta_3$ by CNBr cleavage, the three glycosylated fragments $\beta_3$[23−118], $\beta_3$[388−535], and $\beta_3$[627−701] appear as candidate fragments for encompasing the contact site, although the last two differ by about 4 kDa in size from the experimentally observed band. However, only the first sequence, $\beta_3$[23−118], overlaps with the putative contact site $\beta_3$[109−125] obtained from the enzymatic digestions. Combining these results, we further refined the contact site boundaries to the region $\beta_3$[109−118]. Figure 5 displays the corresponding region on the theoretical digestion maps in which all fragments are represented and superimposed. Region $\beta_3$-[109−118] is the smallest sequence to contain the cross-linking site of [Bpa[28]]echistatin, consistent with limits defined by the pattern of overlapping fragments encompassing the site of ligand photo-cross-linking to the integrin.

*Identification of the Binding Site for RGD-containing ligands in the $\alpha_V\beta_3$ Integrin.* The availability of the structural features of both the receptor (the crystal structure of the extracellular fragment of $\alpha_V\beta_3$ (*10*)) and ligand (NMR structure of echistatin; *26*, *36*) allows placement of the contact sites identified by PAS studies in a three-dimensional context. Using these structures as starting points and the contact sites as structural constraints, possible ligand−receptor interactions were examined by molecular modeling. In the X-ray structure of the receptor, the distance between the cross-linking domains $\beta_3$[167−171] (identified for **2**) and $\beta_3$[109−118] (identified for **1** and **7**) is calculated to have the upper limit of 20 Å, based on the side-chain of M118 of $\beta_3$, the residue closest to $\beta_3$[167−171]. Guided by these contact points, the RGD-containing loop of echistatin was placed in this region, with Lys[21] in echistatin projecting toward the loop containing $\beta_3$[167−171], and Met[28] in echistatin directed to M118, adjacent to the MIDAS domain in $\beta_3$. The C-terminus of echistatin was rotated away from the RGD loop of the ligand, to allow its placement in proximity to the $\beta$-strand containing $\beta_3$[209−220], consistent with the previously reported contact site for K[45](BP)-echistatin (*30*) (Figure 6A). During the simulations, the $\beta$-hairpin of echistatin, which contains RGD, undergoes a conformational change: it opens up, with each strand of the hairpin interacting with the integrin receptor rather than with each other (Figure 6B). This opening up of the $\beta$-hairpin fulfills the photoaffinity cross-linking constraints and places the RGD sequence in very close proximity to the MIDAS. During the simulations, the integrin receptor structure undergoes only slight modifications, ranging from 0.7 to 2.1 Å, with most of the changes well removed from this site. Considering the manual placement of the C-terminus of echistatin and the conformational change of the $\beta$-hairpin, the root-mean-square deviation (RMSD) for the ligand is over 6 Å. Including only the backbone atoms of Lys[21]−Met[28] of echistatin, the RMSD is 3.1 Å (see Figure 6B). Importantly, the opening of the $\beta$-hairpin does not disrupt the disulfide bonds of echistatin. In fact, two of the disulfide bonds (Cys[20]−Cys[39] and Cys[7]−Cys[32]) help stabilize the "squashed" bound form of the ligand, certainly limiting the conformational change to the RGD-containing loop. On the basis of the simulation results, a number of ligand/receptor contacts are observed. Both of the side chains of Arg[24] and Asp[26] in the echistatin RGD triad are in close proximity to the MIDAS in the A-domain of $\beta_3$, made up of D119, S121, and S123. The side chain of Lys[21], N-terminal to the RGD triad in echistatin, is found to interact with E121 and D148 of the $\alpha$-domain of $\alpha_V\beta_3$. In addition, a very hydrophobic pocket formed by Y116, M118, L333, and V340 of $\beta_3$ is found for Met[28] in echistatin.

## DISCUSSION

Unfortunately, high-resolution methods such as nuclear magnetic resonance and X-ray crystallography are not applicable as general tools to gain insight into the structural

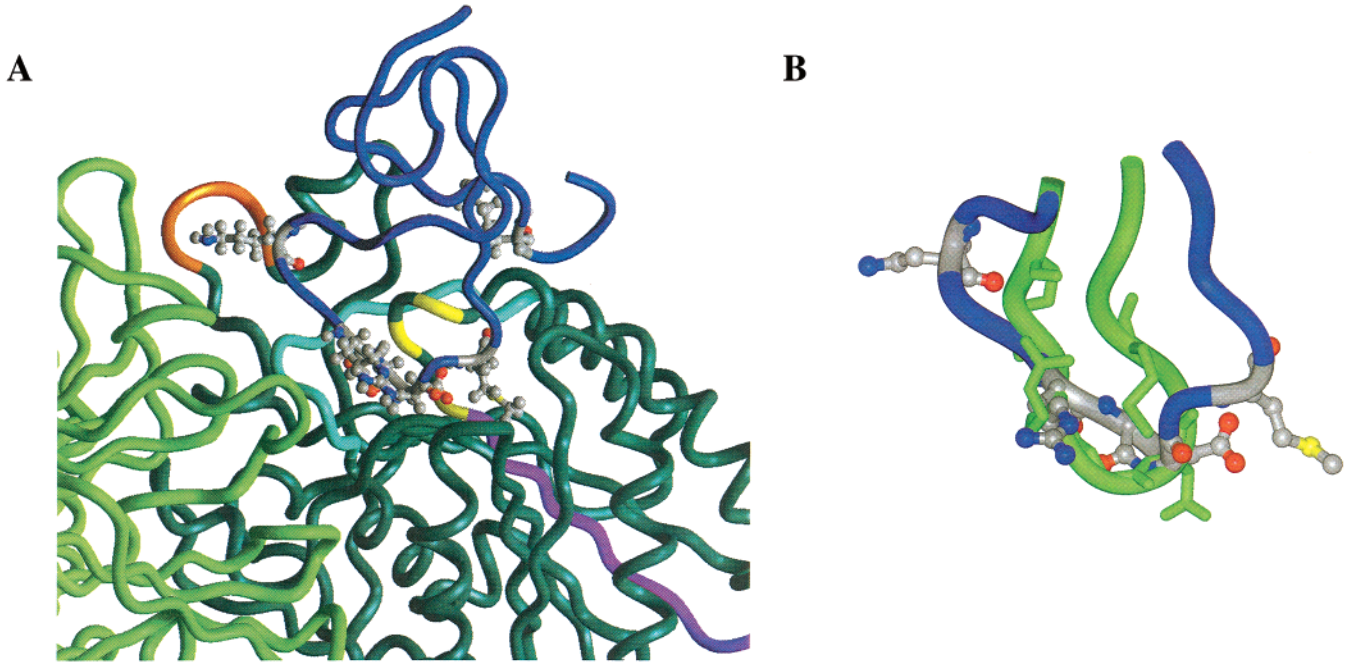


FIGURE 6: (A) Illustration of the model of the binding site of echistatin in $\alpha_V\beta_3$. The integrin receptor is shown in green ($\alpha_V$ light green, $\beta_3$ dark green). The regions of $\beta_3$ identified as contact points are denoted in pink ($\beta_3$[109−118]), orange ($\beta_3$[167−171]), and light blue ($\beta_3$[209−220]). The D119, S121, and S123 forming the MIDAS are denoted in yellow. Echistatin is shown in dark blue, with $Lys^{21}$, $Arg^{24}$−Gly−$Asp^{26}$, $Met^{28}$, and $Lys^{45}$ illustrated in ball-and-stick. The RGD motif is in close proximity and in an antiparallel orientation to the MIDAS. (B) Superposition of the RGD-containing loop of echistatin from the NMR-derived structure (green) and the resulting structure from MD simulations employing the echistatin/$\alpha_V\beta_3$ contact points derived from photoaffinity cross-linking (dark blue). The residues $Lys^{21}$, $Arg^{24}$−Gly−$Asp^{26}$, and $Met^{28}$ are displayed. The simulations suggest that the $\beta$-hairpin loop of echistatin opens up during the interaction with the intergrin receptor.

details of bimolecular interactions between ligands and their cognate membrane-embedded receptors. Therefore, the PAS approach employed in this study is almost the only one that allows characterizing directly the ligand−receptor bimolecular interface. SDS−PAGE analysis of consecutive and specific chemical and enzymatic digestions of the photo-cross-linked ligand−receptor conjugate combined with the specific fragmentation patterns, revealed from the theoretical restriction digestion maps of the human $\beta_3$-subunit, identifies the relevant bimolecular contact sites with a high degree of confidence (*13*−*23*, *30*).

Our study aims to identify echistatin−$\alpha_V\beta_3$ bimolecular interactions in proximity to the RGD triad of echistatin and compare them with those of small cyclic RGD-containing peptides in order to identify the binding site in $\alpha_V\beta_3$ for the RGD motif. Echistatin binds to $\beta_3$ subunit containing integrins with high affinity compared to small cyclic RGD-containing ligands (*27*). Marcinkiewicz and co-workers concluded from their structure−activity studies of echistatin that the shape of the RGD loop is responsible for selective recognition among integrin receptor subtypes, whereas the C-terminus is involved in binding to the resting form of the receptor and induction of significant conformational changes in the receptor (*28*). We therefore designed echistatin analogues **5** and **7**, which contain a single Bpa residue (positions 21 and 28, respectively) in positions corresponding to the positions of the Bpa residues relative to the RGD triad in the cyclic heptapeptide ligands **1** and **2** (Table 1). In the third analogue (**6**), incorporation of $Bpa^{23}$ placed the photoreactive moiety immediately N-terminal to RGD, therefore allowing the identification of a contact site in close proximity to the RGD motif. Our previous attempts to incorporate a photophore directly within the RGD triad disrupted ligand binding to the vitronectin receptor (*37*). Together, these analogues have the potential to identify the contact sites within $\alpha_V\beta_3$ for RGD, the recognition motif present in many endogeneous ligands for integrins.

The substitution of Leu in echistatin for $Met^{28}$ in both [$Bpa^{21}$,$Leu^{28}$]- and [$Bpa^{23}$,$Leu^{28}$]echistatin (**5** and **6**, respectively) is aimed at protecting these analogues from CNBr cleavage, a generic approach to maintaining the connectivity between the position of conjugation (21 and 23) and the radiolabeled $Tyr^{31}$ in the ligand−receptor photoconjugated fragments generated during the analysis. In addition, the substitution of the $Met^{28}$ residue in these peptides prevents potential oxidation at this position, which was previously shown to cause a dramatic decrease in affinity toward the $\alpha_V\beta_3$ receptor (*38*). McLane and co-workers reported that [$Leu^{28}$]echistatin is a potent $\alpha_V\beta_3$ receptor agonist (*39*). Indeed, we found [$Leu^{28}$]echistatin and its Bpa-substituted analogues to have high affinity for the recombinant human $\alpha_V\beta_3$ receptor (Figure 1).

Our previous PAS studies, as well as various other studies, identified the common $\beta_3$ subunit of integrins $\alpha_V\beta_3$ and $\alpha_{IIb}\beta_3$ as the major binding site for RGD-containing ligands (*22*, *23*, *30*, *37*, *40*−*45*). Nevertheless, the two receptors differ in their tissue distribution, physiological functions, and involvement in pathophysiological states (*46*, *47*). Apparently, the presence of two different $\alpha$ subunits and their differential interaction with the $\beta_3$ subunit generates distinct ligand specificities for these closely related receptors (*28*, *40*, *48*). The comparative binding of the novel BP-containing echistatin analogues is in general agreement with previous reports (*28*, *48*), demonstrating that modifications around the

Table 1: Summary of RGD-Containing Ligands Used for Photoaffinity Cross-Linking Studies and the Contact Sites Identified on the $\alpha_V\beta_3$ Integrin[a]

| RGD-containing ligand | Cross-linking site in $\alpha_V\beta_3$ | Ref. |
|---|---|---|
| $^{125}$I-BH-Ahx-Cys-Asn-Dmt-Arg-Gly-Asp-Cys-**Bpa**-$NH_2$ (*1*) | $\beta_3$[99-118] | (23) |
| ***p*Bz$_2$**-Cys-Asn-Dmt-Arg-Gly-Asp-Cys-N$^\epsilon$-($^{125}$I-BH-Ahx)Lys-$NH_2$ (*2*) | $\beta_3$[167-171] | (22) |
| $^{125}$I-BH-Ahx-Cys- Lys(N$^\epsilon$-***p*Bz$_2$**)-Dmt-Arg-Gly-Asp-Cys-$NH_2$ (*3*) | $\alpha_V$, $\beta_3$ | (37) |
| $^{125}$**I**-[Arg$^{35}$,Lys$^{45}$(N$^\epsilon$-***p*Bz$_2$**)]echistatin (*4*) | $\beta_3$[209-220] | (30) |
| [**Bpa**$^{21}$,Leu$^{28}$]echistatin (*5*) | $\alpha_V$, $\beta_3$ | t.m. |
| [**Bpa**$^{23}$,Leu$^{28}$]echistatin (*6*) | $\beta_3$ | t.m. |
| [**Bpa**$^{28}$]echistatin (*7*) | $\beta_3$[109-118] | t.m. |

[a] Compounds **1**−**4** were the target of previous studies. In all structures, the photoreactive benzophenone moieties, either Bpa or *p*Bz$_2$, are in bold. Abbreviations: Ahx, 6-aminohexanoic acid; BH, Bolton-Hunter reagent; Dmt, 5,5-dimethylthiazolidine-carboxylic acid; t.m., this manuscript.

RGD motif in echistatin differentially affect the binding affinities for $\alpha_V\beta_3$ versus $\alpha_{IIb}\beta_3$ integrins. Specifically, the three Bpa-substituted echistatin analogues maintain a high binding affinity for the $\alpha_V\beta_3$ receptor but show no significant binding for the $\alpha_{IIb}\beta_3$ receptor. Consequently, the cross-linking efficiencies to the $\alpha_{IIb}\beta_3$ receptor are poor: only [Bpa$^{23}$]echistatin (**6**) generates a detectable $\beta_3$-derived band after cross-linking. These results provide further evidence that the $\alpha$ subunit contributes to ligand−receptor interactions. This function of the $\alpha$-subunit is consistent with the now available crystal structure of the ectopic portion of the $\alpha_V\beta_3$ receptor: the $\alpha$ subunit is in immediate proximity to the A-domain in $\beta_3$ (*10*). It is the A-domain in the $\beta_3$ subunit that was shown previously to be involved in binding RGD-containing ligands through interactions with the integrin's MIDAS (*11*, *49*−*52*).

The much higher cross-linking efficiency of [Bpa$^{23}$,Leu$^{28}$]-echistatin (**6**) compared to the Bpa$^{21}$- and the Bpa$^{28}$-containing analogues (**5** and **7**, respectively) (Figure 2A) is unexpected since the binding affinity of the three analogues is similar (see Figure 1). The increased cross-linking suggests either a close proximity between Bpa$^{23}$ and a very reactive insertion site in the receptor binding pocket or an especially tight local interaction between Bpa$^{23}$ and an insertion site resulting from the immediate proximity of the photophore to the principal binding epitope, the RGD triad. In support of the former mechanism, our molecular model of the echistatin−$\alpha_V\beta_3$ ectopic domain complex shows that the side-chain of Ala$^{23}$ of echistatin is only 10 Å removed from the potential highly favored photoinsertion sites M165 and M186 of $\beta_3$.

The 10-amino-acid segment $\beta_3$[109−118] that contains the contact site for position 28 in [Bpa$^{28}$]echistatin (**7**) is included within the previously identified contact domain for the Bpa residue in the heptapeptide ligand **1**, $\beta_3$[99−118] (*22*). Since the Bpa residues in **7** and **1** are located in the same position relative to the RGD triad, namely −RGD−X−Bpa−, the sequence $\beta_3$[109−118] represents a considerable refinement of the boundaries for the contact site of a residue removed two positions from the carboxyl end of the RGD triad in the ligand.

In analogous fashion, in both [Bpa$^{21}$,Leu$^{28}$]echistatin (**5**) and the cyclic heptapeptide **2**, the photophore is located three positions N-terminal to the RGD triad (i.e., BP−X−X−RGD). In this study, we observe cross-linking of the echistatin photoreactive analogue **5** to both the $\alpha_V$ and the $\beta_3$ chains, with a higher yield to the former one. This finding is in contrast to our previous observations with BP-substituted RGD-containing ligands, as well as the cross-linking studies of others, all of which report almost exclusive cross-linking to the $\beta_3$ subunit (*22*, *23*, *30*, *37*, *43*, *44*). This difference in cross-linking may be due to differences in probes, especially in the presentation of the BP photoreactive moiety. The cross-linking of [Bpa$^{21}$,Leu$^{28}$]echistatin (**5**) to both $\alpha_V$ and $\beta_3$ subunits indicates that, during ligand binding, the amino acid at position 21 is in close proximity to the interface of both subunits. The cyclic heptapeptide **2** cross-links to a site included in the $\beta_3$[167−171] loop. In the crystal structure of the ectopic portion of $\alpha_V\beta_3$, this loop is located immediately adjacent to the $\beta$-propeller of the $\alpha_V$ chain (Figure 6A) (*10*). The reduced flexibility of the BP in the cyclic heptapeptide structure may restrict photoinsertion almost

exclusively to the $\beta_3$ subunit. In addition, there is a subtle distinction in the presentation of the BP in echistatin versus the cyclic hexapeptide. While BP is presented on a side chain in **5**, it is presented as a short extension of the backbone (a $N^{\alpha}$-*p*-benzoylbenzoyl) in **2**. The more extended and conformationally flexible BP moiety in the echistatin analogue permits photoinsertion at sites in both the $\alpha_V$ and the $\beta_3$ subunits. Therefore, the $Bpa^{21}$ probe offers access to the $\alpha_V$ interface for the first time.

Interestingly, we have previously noted that the cyclic heptapeptide ligand **3** (Table 1), in which the BP moiety is located on the $\epsilon$-amino group of a lysyl side-chain, one residue removed from the N-terminal side of RGD, also cross-links to both $\alpha_V$ and $\beta_3$ subunits, although with low efficiencies (*37*). Taken together, we conclude that positioning the photoreactive moieties in close proximity to the RGD motif allows probing the RGD-binding cleft, which is either part of or in close proximity to the $\alpha_V-\beta_3$ interface located in the "head" of the ectopic domain of $\alpha_V\beta_3$ (*10*).

The shortest distance between the two identified cross-linking regions, $\beta_3$[167−171] and $\beta_3$[109−118], calculated from the crystal structure is about 20 Å (taking into account the side-chain of M118, the closest residue to the $\beta_3$[167−171] loop). A distance of 20 Å corresponds to the maximal distance between two BP moieties separated by six amino acid residues, as is the separation between the BP moiety in BP-X−X-RGD (e.g., ligand *5*) and the BP moiety in −RGD−X−BP (e.g., ligands **1** and **7**). Therefore, one may conclude that the most probable photoinsertion site for the BP moiety in echistatin analogue **7** is M118 located at the carboxyl end of the $\beta_3$[109−118] contact domain. It is important to note that methionine is a highly reactive site for BP photoinsertion and is often found as an actual contact point (*13*, *14*, *16*, *53*−*57*).

Consistent with such an orientation of RGD-containing ligands is the auxiliary contact site identified previously for $K^{45}$(BP)-echistatin (*30*). As evident from the crystal structure, the $\beta_3$[209−220] region, which contains the contact site for the BP moiety in position 45, is accessible to the C-terminal part of echistatin when oriented in such a way that positions 21 and 28 in echistatin are also making contact as described above.

The modeling of the $\alpha_V\beta_3$−echistatin complex (see Figure 6) shows how the RGD-containing ligand fits into the binding pocket, placing position 21 in echistatin close to the cross-linking region $\beta_3$[167−171] (identified for **2**) and position 28 close to the M118 of $\beta_3$ (identified for **1** and **7**). The RGD motif is thereby brought in close proximity and in an antiparallel orientation to the MIDAS residues in the integrin thought to be important in ligand-binding (*11*, *49*, *52*, *58*, *59*). The simulations indicate that the $\beta$-hairpin loop of echistatin, which presents the RGD motif, opens up and expands upon interaction with the integrin receptor, fulfilling experimental observations without imposing major conformational changes of the receptor. Future PAS studies with [$Bpa^{21}$]- and [$Bpa^{23}$]echistatin analogues should help to establish more fully the identity of binding sites for echistatin and small RGD-containing ligands.

Whether the highly bent X-ray structure of the ectopic domain of $\alpha_V\beta_3$, which was obtained in the presence of $Ca^{2+}$ but in the absence of $Mg^{2+}$ and $Mn^{2+}$, represents the active ligand-binding state (*10*) remains an open question. According to Beglova and co-workers, who studied the integrin−epidermal growth factor-like domain 3 (I-EGF3) of the integrin $\beta_2$ subunit, the active conformation of the ectopic domain is fully extended (*60*). Whatever is the bioactive conformation, we believe that PAS studies, conducted with the intact membrane-embedded receptor in the presence of divalent cations, probe the bimolecular interface between the ligand and the bioactive conformation of the receptor. Therefore, our studies suggest that the identity and spatial disposition of the sites in the A-domain of $\beta_3$ subunit that are in contact with the RGD-containing ligands used in these studies (Figure 6 A) must be very similar in both the active and nonactive conformations.

In conclusion, the model we present describes binding of echistatin, in particular, to the $\alpha_V\beta_3$ integrin. But it may also be a relevant model, in general, for the binding of RGD-containing ligands to integrins. The model was developed by merging experimental data, which identifies contact domains for ligands within the receptor, with data from the recently published crystal structure of the ectopic portion of the $\alpha_V\beta_3$ receptor (*10*). The process we used in generating a model of ligand−integrin binding demonstrates the complementary nature of information obtained from photoaffinity cross-linking studies and X-ray crystallography. Photoaffinity cross-linking provides direct evidence regarding domains of contact between ligand and receptor. The interaction is "frozen" by generating a covalent bond between a known residue in the ligand and an unknown residue in the receptor. While the resolution is not as refined as in X-ray crystal structure, valuable insights can be gained regarding a bimolecular interface as complex as the one studied here, namely, the RGD-containing protein echistatin with the heterodimeric $\alpha_V\beta_3$ integrin. We superimposed this cross-linking data for the receptor when presented in intact cells on the crystal structure of the ectopic portion of $\alpha_V\beta_3$ in isolation from the cellular milieu and in the absence of the ligand. The good agreement between these two sets of data offers strong validation regarding the relevance of the crystal structure of the ectopic portion of $\alpha_V\beta_3$ to the structure of the intact, membrane-embedded, and activated integrin in the context of a cellular environment. At the same time, knowledge of the crystal structure of $\alpha_V\beta_3$ provides insights into the interface of the $\alpha_V$ and $\beta_3$ chains, which is critically important to interpreting photo-cross-linking data and docking the RGD motif in the ligand−integrin model.

## REFERENCES


1. Hynes, R. O. (1992) *Cell 69*, 11−25.
2. Pierschbacher, M. D., and Ruoslahti, E. (1984) *Nature 309*, 30−33.
3. Assa-Munt, N., Jia, X., Laakkonen, P., and Ruoslahti, E. (2001) *Biochemistry 40*, 2373−2378.
4. Lakkakorpi, R., Horton, M. A., Helfrich, M. H., Karhukorpi, E.-K., and Vaananen, H. K. (1991) *J. Cell Biol. 115*, 1179−1186.
5. Horton, M. A., Taylor, M. L., Arnett, T. R., and Helfrich, M. H. (1991) *Exp. Cell Res. 195*, 368−375.
6. Chambers, T. J., Fuller, K., Darby, J. A., and Pringle, J. A. (1986) *Bone Miner. 1*, 127−135.
7. Fisher, J. E., Caulfield, M. P., Sato, M., Quartuccio, H. A., Gould, R. J., Garsky, V. M., Rodan, G. A., and Rosenblatt, M. (1993) *Endocrinology 132*, 1411−1413.
8. Engleman, V. W., Nickols, G. A., Ross, F. P., Horton, M. A., Griggs, D. W., Settle, S. L., Ruminski, P. G., and Teitelbaum, S. L. (1997) *J. Clin. Invest. 99*, 2284−2292.

9. Eliceiri, B. P., and Cheresh, D. A. (1999) *J. Clin. Invest. 103*, 1227−1230.
10. Xiong, J. P., Stehle, T., Diefenbach, B., Zhang, R., Dunker, R., Scott, D. L., Joachimiak, A., Goodman, S. L., and Arnaout, M. A. (2001) *Science 294*, 339−345.
11. Tozer, E. C., Liddington, R. C., Sutcliffe, M. J., Smeeton, A. H., and Loftus, J. C. (1996) *J. Biol. Chem. 271*, 21978−21984.
12. Williams, K. P., and Shoelson, S. E. (1993) *J. Biol. Chem. 268*, 5361−5364.
13. Bisello, A., Adams, A., Mierke, D., Pellegrini, M., Rosenblatt, M., Suva, L., and Chorev, M. (1998) *J. Biol. Chem. 273*, 22498−22505.
14. Greenberg, Z., Bisello, A., Mierke, D. F., Rosenblatt, M., and Chorev, M. (2000) *Biochemistry 39*, 8142−8152.
15. Rolz, C., Pellgrini, M., and Mierke, D. F. (1999) *Biochemistry 38*, 6397−6405.
16. Gensure, R. C., Carter, P. H., Petroni, B. D., Juppner, H., and Gardella, T. J. (2001) *J. Biol. Chem. 276*, 42693−42699.
17. Phalipou, S., Seyer, R., Cotte, N., Breton, C., Barberis, C., Hibert, M., and Mouillac, B. (1999) *J. Biol. Chem. 274*, 23316−23327.
18. Dong, M., Wang, Y., Hadac, E. M., Pinon, D. I., Holicky, E. L., and Miller, L. J. (1999) *J. Biol. Chem. 274*, 19161−19167.
19. Dong, M., Asmann, Y. W., Zang, M., Pinon, D. I., and Miller, L. J. (2000) *J. Biol. Chem. 275*, 26032−26039.
20. Coulie, B., Matsuura, B., Dong, M., Hadac, E. M., Pinon, D. I., Feighner, S. D., Howard, A. D., and Miller, L. J. (2001) *J. Biol. Chem. 276*, 35518−35522.
21. Ji, Z., Hadac, E. M., Henne, R. M., Patel, S. A., Lybrand, T. P., and Miller, L. J. (1997) *J. Biol. Chem. 272*, 24393−24401.
22. Bitan, G., Scheibler, L., Greenberg, Z., Rosenblatt, M., and Chorev, M. (1999) *Biochemistry 38*, 3414−3420.
23. Bitan, G., Scheibler, L., Mierke, D. F., Rosenblatt, M., and Chorev, M. (1999) *Biochemistry 39*, 11014−11023.
24. Gan, Z.-R., Gould, R. J., Jacobs, J. W., Friedman, P. A., and Polokoff, M. A. (1988) *J. Biol. Chem. 263*, 19827−19832.
25. Chen, Y., Pitzenberger, S. M., Garsky, V. M., Lumma, P. K., Sanyal, G., and Baum, J. (1991) *Biochemistry 30*, 11625−11636.
26. Saudek, V., Atkinson, R. A., Lepage, P., and Pelton, J. T. (1991) *Eur. J. Biochem. 202*, 329−338.
27. Garsky, V. M., Lumma, P. K., Friedinger, R. M., Pitzenberger, S. M., Randall, W. C., Veber, D. F., Gould, R. J., and Friedman, P. A. (1989) *Proc. Natl. Acad. Sci. U.S.A. 86*, 4022−4026.
28. Marcinkiewicz, C., Vijay-Kumar, S., McLane, M. A., and Niewiarowoski, S. (1997) *Blood 90*, 1565−1575.
29. Wright, P. S., Saudek, V., Owen, T. J., Harbeson, S. L., and Bitonti, A. J. (1993) *Biochem. J. 293*, 263−267.
30. Scheibler, L., Mierke, D. F., Bitan, G., Rosenblatt, M., and Chorev, M. (2001) *Biochemistry 40*, 15117−15126.
31. Kaiser, E., Colescott, R. L., Bossinger, C. D., and Cook, P. I. (1970) *Anal. Biochem. 34*, 595−598.
32. Bolton, A. E. (1986) *Methods Enzymol. 124*, 18−29.
33. Greenberg, Z., Stoch, S., Traianedes, K., Teng, H., Rosenblatt, M., and Chorev, M. (1999) *Anal. Biochem. 266*, 153−164.
34. Houmard, J., and Drapeau, G. R. (1972) *Proc. Natl. Acad. Sci. U.S.A. 69*, 3506−3509.
35. Horton, M. A. (1997) *Int. J. Biochem. Cell. Biol. 29*, 721−725.
36. Baumann, B. D., and Wronski, T. J. (1995) *Bone 16*, 247−253.
37. Bitan, G., Scheibler, L., Tang, H., Rosenblatt, M., and Chorev, M. (2000) *J. Peptide Res. 55*, 181−194.
38. Kumar, C. C., Nie, H., Rogers, C. P., Malkowski, M., Maxwell, E., Catino, J. J., and Armstrong, L. (1997) *J. Pharm. Exp. Ther. 283*, 843−853.
39. McLane, M. A., Vijay-Kumar, S., Marcinkiewicz, C., Calvete, J. J., and Niewiarowoski, S. (1996) *FEBS Lett. 391*, 139−143.
40. Suehiro, K., Smith, J. W., and Plow, E. F. (1996) *J. Biol. Chem. 271*, 10365−10371.
41. Santoro, S., and Lawing, W. J., Jr. (1987) *Cell 48*, 867−873.
42. Smith, J. W., and Cheresh, D. A. (1990) *J. Biol. Chem. 265*, 2168−2172.
43. Smith, J. W., and Cheresh, D. A. (1988) *J. Biol. Chem. 263*, 18726−18731.
44. Calvete, J. J., McLane, M. A., Stewart, G. J., and Niewiarowski, S. (1994) *Biochem. Biophys. Res. Comm. 202*, 135−140.
45. D'Souza, S. E., Ginsberg, M. H., Burke, T. A., and Plow, E. F. (1990) *J. Biol. Chem. 265*, 3440−3446.
46. Krissansen, G. W. (2000) Integrins: Signaling and Disease, in *Encyclopedia of Life Sciences*, pp 1−10, Nature Publication Group, London.
47. Krissansen, G. W. (2000) Integrin Superfamily, in *Encyclopedia of Life Sciences* pp 1−10, Nature Publishing Group, London.
48. Sato, M., Garsky, V., Majeska, R. J., Einhorn, T. A., Murray, J., Tashjian, A. H., Jr., and Gould, R. J. (1994) *J. Bone Min. Res. 9*, 1441−1449.
49. Bajt, M. L., and Loftus, J. C. (1994) *J. Biol. Chem. 269*, 20913−20919.
50. Lee, J. O., Rieu, P., Arnaout, M. A., and Liddington, R. (1995) *Cell 80*, 631−638.
51. Tuckwell, D. S., and Humphries, M. J. (1997) *FEBS Lett. 400*, 297−303.
52. Lin, E. C. K., Ratnikov, B. I., Tsai, P. M., Gonzalez, E. R., McDonald, S., Pelletier, A. J., and Smith, J. W. (1997) *J. Biol. Chem. 272*, 14236−14243.
53. Kage, R., Leeman, S. E., Krause, J. E., Costello, C. E., and Boyd, N. D. (1996) *J. Biol. Chem. 271*, 25797−25800.
54. Girault, S., Sagan, S., Bolbach, G., Lavielle, S., and Chassaing, G. (1996) *Eur. J. Biochem. 240*, 215−222.
55. Behar, V., Bisello, A., Rosenblatt, M., and Chorev, M. (1999) *Endocrinology 140*, 4251−4261.
56. Li, H., Macdonald, D. M., Hronowski, X., Costello, C. E., Leeman, S. E., and Boyd, N. D. (2001) *J. Biol. Chem. 276*, 10589−10593.
57. Egnaczyk, G. F., Greis, K. D., Stimson, E. R., and Maggio, J. E. (2001) *Biochemistry 40*, 11706−11714.
58. Loftus, J. C., O'Toole, T. E., Plow, E. F., Glass, A., Frelinger 3d., A. L., and Ginsberg, M. H. (1990) *Science 249*, 915−918.
59. Bajt, M. L., Ginsberg, M. H., Frelinger, A. L., Berndt, M. C., and Loftus, J. C. (1992) *J. Biol. Chem. 267*, 3789−3794.
60. Beglova, N., Blacklow, S. C., Takagi, J., and Springer, T. A. (2002) *Nat. Struct. Biol. 9*, 282−287.


BI025690T